Ion-Pair Dissociation Dynamics of Cl_2: Adiabatic State Correlation

Chang Zhou, Yusong Hao, and Yuxiang Mo*

Department of Physics and Key Laboratory for Atomic and Molecular Nanosciences, Tsinghua University, Beijing, 100084, China

Received: May 14, 2008; Revised Manuscript Received: June 28, 2008

The ion-pair dissociation dynamics of $Cl_2 \xrightarrow{XUV} Cl^-(^1S_0) + Cl^+(^3P_{2,1,0})$ in the range 12.41−12.74 eV have been studied employing coherent extreme ultraviolet (XUV) radiation and the velocity map imaging method. The ion-pair yield spectrum has been measured, and 72 velocity map images of $Cl^-(^1S_0)$ have been recorded for the peaks in the spectrum. From the images, the branching ratios among the three spin−orbit components $Cl^+(^3P_2)$, $Cl^+(^3P_1)$ and $Cl^+(^3P_0)$ and their corresponding anisotropic parameters β have been determined. The ion-pair dissociation mechanism is explained by predissociation of Rydberg states converging to ion-core $Cl_2^+(A^2\Pi_u)$. The $Cl^-(^1S_0)$ ion-pair yield spectrum has been assigned based on the symmetric properties of Rydberg states determined in the imaging experiments. The parallel and perpendicular transitions correspond to the excitation to two major Rydberg series, $[A^2\Pi_u]3d\pi_g,^1\Sigma_u^+$ and $[A^2\Pi_u]5s\sigma_g,^1\Pi_u$, respectively. For the production of $Cl^+(^3P_0)$, it is found that all of them are from parallel transitions. But for $Cl^+(^3P_1)$, most of them are from perpendicular transitions. The production of $Cl^+(^3P_2)$ is the major channel in this energy region, and they come from both parallel and perpendicular transitions. It is found that for most of the predissociations the projection of the total electronic angular momentum on the molecular axis (Ω) is conserved. The ion-pair dissociation may be regarded as a probe for the symmetric properties of Rydberg states.

I. Introduction

The ion-pair states have some interesting properties in comparison with the covalent states.[1−13] For example, the long-range potential in the ion-pair converges as $1/r$ that makes strong ionic bonds of ion-pair states. The threshold for ion-pair dissociation is usually higher than or comparable to the ionization energy of molecules.[7−10] High density of Rydberg states converging to ion-core with electronic excited states or ground states exists in this energy region. Strong nonadiabatic interactions in dissociation or avoided crossings between the potential energy curves of Rydberg states and ion-pair states occur. The dissociation dynamics that involves the coupling between the ion-pair states and Rydberg states is strongly dependent on the excitation photon energies, which is very different from photodissociation of small molecules in the lower excited states or covalent states. Therefore, the ion-pair dissociation provides us a probe for the properties of electronic excited states with energies higher than the ionization energies of molecules, or the so-called superexcited state.[1−3] The chlorine molecule is one of the benchmark molecules for studying the electronic structures and photochemistry of diatomic molecules.[10−22] Its ion-pair dissociation dynamics should provide us great insights into the interaction between Rydberg states and ion-pair states.

Berkowitz et al. have studied the ion-pair dissociation of Cl_2 by measuring the Cl^- ion-pair yield spectrum using XUV radiation from both the hydrogen many-line spectrum and the Hopfield continuum of helium with a resolution of 0.14 (Å).[22] Their observed spectrum consists of four distinct bands from 105 to 75 nm. The two lowest bands correlate with $Cl^-(^1S_0) + Cl^+(^3P_j)$ in energy, and the other two were inferred by them to have asymptotes of $Cl^-(^1S_0) + Cl^+(^1D_2)$ and $Cl^-(^1S_0) + Cl^+(^1S_0)$, respectively. Recently, using velocity map imaging[23] and tunable XUV laser, we have studied the ion-pair dissociation dynamics of Cl_2 in the range 13.26−13.73 eV corresponding to the third band of Berkowitz et al.[11,22] Two dissociation channels corresponding to $Cl^-(^1S_0) + Cl^+(^3P_j)$ and $Cl^-(^1S_0) + Cl^+(^1D_2)$ have been observed. The dissociation mechanism was explained by the predissociation of Rydberg states converging to the ion-core $Cl_2^+(A^2\Pi_u)$. The main channels are from the perpendicular transitions correlating with the production of $Cl^+(^1D_2)$ from the predissociations of Rydberg states, $[A^2\Pi_u]ns\sigma_g,^1\Pi_u$ ($n = 6, 7$) by ion-pair state $2^1\Pi_u(^1D_2)$. Here, $[A^2\Pi_u]$ designates the ion-core. The parallel transitions for the production of $Cl^+(^1D_2)$ were also observed, and were proposed to be from the predissociations of $[A^2\Pi_u]nd\pi_g,^1\Sigma_u^+$ ($n = 4, 5$) and the nonadiabatic interactions among $1^1\Sigma_u^+(^1D_2)$, $0_u^+(^3P_2)$ and $0_u^+(^3P_0)$. For fragments $Cl^+(^3P_j)$, it was found that both parallel and perpendicular transitions occur. However, due to the large available energies for the dissociation, we could not resolve completely the three spin−orbit components. Therefore, some of the important questions about the dissociation dynamics have not been answered in our previous work.[11] For example, according to the adiabatic theory, fragments $Cl^+(^3P_0)$ and $Cl^+(^3P_1)$ could only come from the parallel and perpendicular transitions, respectively. However, these conclusions are not true if nonadiabatic interactions involving the so-called heterogeneous perturbation play an important role in the dissociation. The branching ratios among the three spin−orbit components should be also interesting for understanding the coupling between the ion-pair states and Rydberg states.

In this work, we will report our studies on the ion-pair dissociation of Cl_2 in the energy range of 12.41−12.74 eV using velocity map imaging and XUV laser, which corresponds to the second band of Berkowitz et al.[22] The ion-pair yield

* To whom correspondence should be addressed. E-mail: ymo@mail.tsinghua.edu.cn.

10.1021/jp804272w CCC: $40.75
Published on Web 08/14/2008

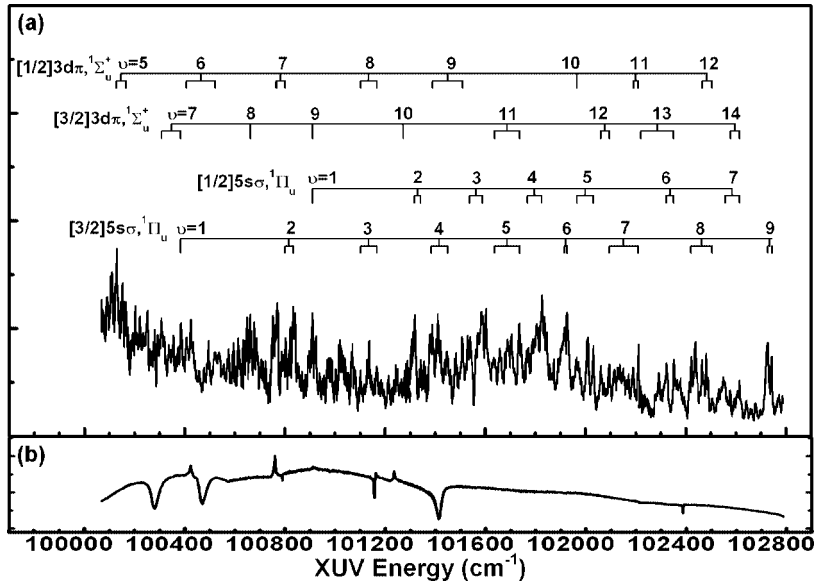

Figure 1. (a) $^{35}Cl^-$ ion-pair yield spectrum: $Cl_2 + h\nu \rightarrow {}^{35,37}Cl^+(^3P_j) + {}^{35}Cl^-(^1S_0)$ under zero electric field, an extraction field ~700 V/cm was exerted after a delay of ~300 ns relative to the XUV laser pulse. The $^{35}Cl^-$ signal intensities have not been normalized to the XUV light intensities due to the large fluctuations of the light intensities with the photon energies. The Rydberg state assignments are also shown, υ is the vibrational quantum number of $Cl_2^+(A^2\Pi_u)$. (b) The XUV light intensities as function of photon energies. It is noted that there is no appreciable difference between the ion pair yield spectra under the electric field and under the field free condition in this energy range.

spectrum and 72 velocity map images have been obtained. From the images, the anisotropic parameters for the three spin−orbit components and their branching ratios have been determined. The ion-pair dissociation dynamics is discussed using the predissociation mechanism of Rydberg states and adiabatic state correlation diagram.

II. Experimental Section

The details of our XUV/VUV photoelectron and photoion spectrometer have been described previously, so only a brief summary is given here.[7−11] The coherent XUV radiation was generated using the resonance enhanced four-wave sum mixing ($2\omega_1 + \omega_2$) in a pulsed Xe jet. An Nd:YAG (YAG−yttrium aluminum garnet) (20 Hz) pumped two dye laser system was used in the experiments. One beam produced by tripling the dye-laser frequency was fixed to match the two-photon resonance ($2\omega_1$) frequency of the Xe $5p^5(^2P_{3/2})6p[1/2]_0 \leftarrow (5p^6)^1S_0$ transition at 80118.96 cm^{-1}. The other dye laser was tuned from 440 to 500 nm.

The apparatus consists of four vacuum chambers: (A) frequency mixing chamber, which houses a pulsed Xe jet (diameter = 1 mm); (B) monochromator chamber, which houses a gold coated toroidal grating; (C) ionization chamber, which houses an electrostatic lens system for velocity map imaging and a time-of-flight tube equipped with imaging quality dual MCP (microchannel plate) (ø50 mm and a channel pitch of 12 μm, North Night Vision, Nanjing Branch); an MCP detector is also installed in this chamber to monitor the VUV light intensity; (D) molecular beam source chamber, which houses a pulsed valve (orifice diameter = 0.7 mm) to produce a pulse molecular beam. The beam enters the ionization chamber through a skimmer (orifice diameter = 1 mm).

In the measurement of ion-pair yield spectrum, the ion and XUV light signals from MCPs were fed into two identical boxcars (SR 250, Stanford Research Systems), and transferred to a personal computer. To record the ion-pair yield spectrum under zero electric field, a pulsed electric field was used to extract the $^{35}Cl^-$ fragments after a delay of ~300 ns relative to the XUV laser pulses. The electric pulses to synchronize the two pulse valves, the Nd:YAG laser, and the pulsed electric field were provided by two digital delay generators (DG 535, Stanford Research Systems). For imaging experiments, the imaging plane is perpendicular to the molecular beam, and the distance from it to the interaction point between the XUV laser and molecular beam is 85 cm. The mass gate selecting both $^{35}Cl^-$ and $^{37}Cl^-$ was a positive 1500 V pulse of 100 ns width provided by a high voltage pulsed generator (PVM-4140, DEI). The ion images were captured by a deep cooled CCD camera with a resolution of 1024 × 1024 pixel^2 (Andor DU-434). The Cl_2 gas sample was premixed with Kr (Kr 93%, Cl_2 7%), and the stagnation pressure used was about 1000 Torr at room temperature. In the experiments, the pressures for the molecular beam source and ionization chamber were around 3×10^{-5} Torr and 1×10^{-7} Torr, respectively. The rotational temperature of the supersonic cooled Cl_2 beam was less than 10 K. The frequencies of the dye lasers were calibrated using He/Ne and He/Ar optogalvanic lamps. The uncertainties of the XUV photon energies reported in the following are ±1 cm^{-1}.

III. Results and Discussion

A. Ion-Pair Yield Spectrum and Its Assignments. Panel (a) of Figure 1 shows the $^{35}Cl^-$ ion-pair yield spectrum of Cl_2 under zero electric field in the range 100000−102800 cm^{-1}. Figure 2 is an expanded view of Figure 1 with index numbers on peaks at which we have measured images. The $^{35}Cl^-$ signal intensities have not been normalized with the XUV light intensities due to the large fluctuations of light intensities with photon energies. The spectrum of XUV light intensity shown in panel (b) of Figure 1 is mainly determined by the efficiency of the nonlinear four-mixing process. The ion-pair yield spectrum with intensity normalization has been reported previously by Berkowitz et al.[22]

It is noted that there is no appreciable difference between the ion pair yield spectra under the electric field strength of ~700 V/cm and under the field free condition in this energy range. There are two reasons for this. The first is that the applied

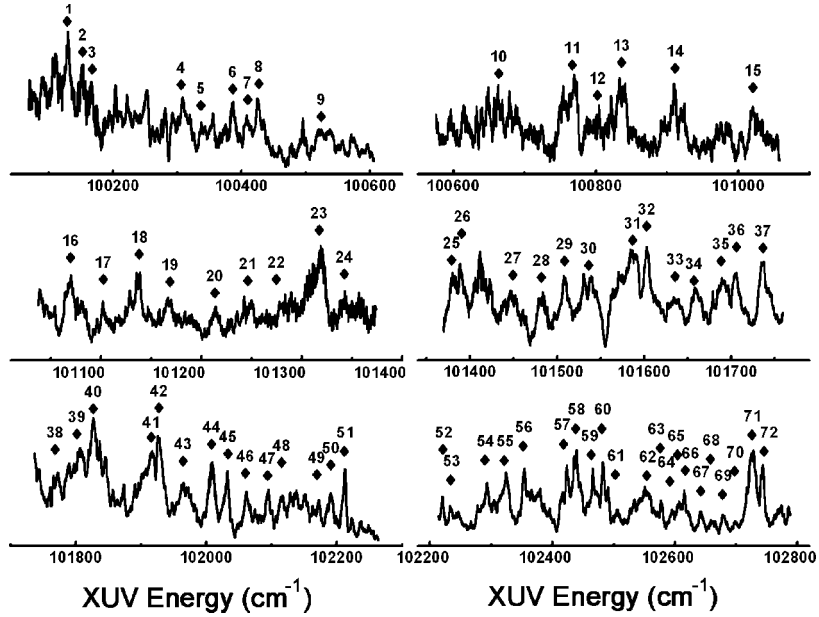

Figure 2. An expanded view of the $^{35}Cl^-$ ion-pair yield spectrum. The symbol ◆ indicates the peak at which an ion image was taken, and the number above it is our index of the image. The photon energy positions, their assignments, and the related dynamical information can be found in Table 2 using the index numbers.

TABLE 1: The Ionization Energy (IE) for the Production of $^{35}Cl_2^+(A^2\Pi_u,v)$ Derived by Combining the Data from the ZEKE Spectrum[10] of Cl_2 and the Emission Spectrum[24] of $^{35}Cl_2^+(A^2\Pi_u \rightarrow X^2\Pi_g)$[a]

	$A^2\Pi_{u,3/2}$			$A^2\Pi_{u,1/2}$		
v	ΔG[b]	$T_0 + G(v)$[c]	IE[d]	ΔG[b]	$T_0 + G(v)$[c]	IE[d]
0	0	20281	112927	0	20256	113621
1	512	20793	113439	347	20603	113968
2	318	21111	113758	346	20950	114314
3	296	21407	114053			

[a] The IEs for higher vibrational states with uncertainties around ±2 cm^{-1} can be found in ref 11. The energy units are cm^{-1}. [b] $\Delta G = G(v) - G(v-1)$, where $G(v)$ represents the vibrational energy for vibrational quantum number v. The data are from the extrapolation and estimated to have uncertainties ~20 cm^{-1}. [c] T_0 is the electronic term energy of $^{35}Cl_2^+(A^2\Pi_{u,3/2})$ or $^{35}Cl_2^+(A^2\Pi_{u,1/2})$ relative to $^{35}Cl_2^+(X^2\Pi_{g,3/2})$ or $^{35}Cl_2^+(X^2\Pi_{g,1/2})$, respectively. [d] The IE represents the ionization energy for the transition $Cl_2^+(A^2\Pi_{u,3/2},v) \leftarrow Cl_2(X^1\Sigma_g^+)$ or $Cl_2^+(A^2\Pi_{u,1/2},v) \leftarrow Cl_2(X^1\Sigma_g^+)$. The IE has an uncertainty of ± 20 cm^{-1}.

photon energy is about 5000 cm^{-1} higher than the threshold for ion-pair production (95443 cm^{-1}),[10] which is much larger than the red shift of the threshold for ion-pair dissociation due to the electric field, $\sim 4\sqrt{E} = 106$ cm^{-1}. The second reason is that the spectrum arises from the predissociation of Rydberg states with low principal quantum numbers, as will be seen in the following discussion.

The ion-pair yield spectrum is characterized by broad background signals overlapped with many resolved structures. Based on this observation, Berkowitz et al. proposed that the ion-pair dissociation should occur via the predissociation of Rydberg states converging to ion-core $(\sigma_g 3p)^2(\pi_u 3p)^3(\pi_g 3p)^4$, $Cl_2^+(A^2\Pi_u)$.[22] The probability for excitation to Rydberg states converging to $Cl_2^+(X^2\Pi_g)$ is low in this energy region since it requires very large principal quantum numbers and also very high vibrational excitations for the Rydberg series, which are unfavorable in the transition intensities.

The assignments for Rydberg states follow the same procedures used in our previous paper.[11] Therefore, only a brief description will be given here. The energy levels of Rydberg series are expressed by

$$E = \mathrm{IE}(v^+) - \frac{\mathrm{Ry}}{(n^*)^2} \quad (1)$$

where Ry is the Rydberg constant for Cl_2, n^* is the effective principal quantum number, and $\mathrm{IE}(v^+)$ is the ionization energy (IE) for the production of $Cl_2^+(A^2\Pi_u)$ at the vth vibrational quantum state.

There is yet no experimentally determined $\mathrm{IE}(v^+)$ reported, however, they can be derived by combining data from the emission spectrum for the transition of $Cl_2^+(A^2\Pi_u \rightarrow X^2\Pi_g)$ and the IEs for $Cl_2^+(X^2\Pi_g)$ from the zero-kinetic energy (ZEKE) photoelectron spectrum of Cl_2, which we obtained recently.[10,24] Unfortunately, the low vibrational states for $Cl_2^+(A^2\Pi_u)$ have not been observed in the emission spectrum. An extrapolation of the data is necessary. The vibrational structure for $Cl_2^+(A^2\Pi_u)$ is found to be very irregular due to the perturbation by its adjacent electronic states. However, it is noted previously that the vibrational states of $Cl_2^+(A^2\Pi_{u,3/2})$ can be divided into three groups, group 1 with $v = 0$, 3, 6, 9, and 12; group 2 with $v = 1$, 4, 7, and 10; group 3 with $v = 2$, 5 and 8.[24] Based on this observation, we obtained the empirical formula for the vibrational energy spacings for groups 1, 2 and 3 by least-squares fitting to the known experimental data. They are $\Delta G(v+1) = 512.2 - 10.8v$, $\Delta G(v+1) = 320.7 - 2.3v$ and $\Delta G(v+1) = 293.7 + v$ for groups 1, 2 and 3, respectively. For $Cl_2^+(A^2\Pi_{u,1/2})$, the empirical formula for vibrational energy spacings obtained by least-squares fitting is $\Delta G(v+1) = 347.3 - 0.8v$. Due to the very irregular vibrational energies for $v = 5$ and 6, the two vibrational states have not been used in obtaining this formula. The vibrational energy spacings calculated using the above formulas are listed in Table 1. The IEs thus obtained for $v = 0$, 1, 2 and 3 for $Cl_2^+(A^2\Pi_{u,3/2})$ and $v = 0$, 1 and 2 for $Cl_2^+(A^2\Pi_{u,1/2})$ are listed in Table 1, and the accuracies for them are estimated to be better than ±20 cm^{-1}, which is good enough for assignment of low n^* Rydberg states. The IEs for higher vibrational states with uncertainties around ±2 cm^{-1} can be found in ref 11.

TABLE 2: Summary of Experimental Results and Assignments for Ion-Pair Dissociation: $Cl_2 + h\nu \rightarrow Cl^+(^3P_j) + Cl^-(^1S_0)$

		branching ratio[c]			$\beta(^3P_j)$[d]			$[A^2\Pi_{u,3/2}]$[e]			$[A^2\Pi_{u,1/2}]$[e]		
no.[a]	XUV energy[b]	$Cl^+(^3P_0)$	$Cl^+(^3P_1)$	$Cl^+(^3P_2)$	$Cl^+(^3P_0)$	$Cl^+(^3P_1)$	$Cl^+(^3P_2)$	nl	n^*	v	nl	n^*	v
1	100128	0.48	0.25	0.27	2.00	0.14	−0.12				3d	2.69	5
2	100150	0.08	0.30	0.62	1.08	−0.40	−0.06						
3	100164	0.15	0.23	0.62	1.77	−0.10	0.31				3d	2.69	5
4	100308	0.13	0.09	0.78	1.78	0.10	1.04	3d	2.68	7			
5	100336		0.43	0.57		0.55	−0.01	3d	2.68	7			
6	100386	0.16	0.31	0.52	1.37	−0.44	0.16	5s(3d)	2.90(2.69)	1(7)			
7	100408	0.28	0.11	0.60	1.80	0.42	1.11				3d	2.67	6
8	100425	0.39	0.17	0.44	2.00	0.30	0.47				3d	2.67	6
9	100524	0.37	0.10	0.54	1.80	0.46	0.25				3d	2.68	6
10	100664	0.35		0.65	2.00		1.30	3d	2.68	8			
11	100766			1.00			0.43				3d	2.67	7
12	100801		0.33	0.67		−0.05	1.03	5s	2.91	2	3d	2.68	7
13	100834		0.25	0.75		−0.42	−0.75	5s	2.91	2			
14	100910	0.23	0.28	0.49	1.54	−0.21	0.04	3d	2.68	9	5s	2.90	1
15	101020	0.19	0.23	0.58	1.40	−0.25	−0.26						
16	101068	0.22	0.24	0.54	1.43	−0.10	−0.48						
17	101102	0.09	0.33	0.58	1.18	−0.05	0.09	5s	2.91	3	3d	2.67	8
18	101137	0.19	0.22	0.59	1.46	−0.10	0.00	5s	2.91	3	3d	2.68	8
19	101167	0.30	0.41	0.29	1.67	−0.27	0.29	5s	2.91	3	3d	2.68	8
20	101214		0.29	0.71		−0.31	−0.27						
21	101246	0.14	0.19	0.68	1.40	−0.16	−0.03						
22	101273	0.19		0.81	1.20		0.40	3d	2.67	10			
23	101317		0.29	0.71		−0.54	−0.78				5s	2.90	2
24	101342		0.33	0.67		−0.20	−0.29				5s	2.91	2
25	101384		0.39	0.61		−0.21	−0.47	5s	2.89	4			
26	101390	0.12	0.34	0.54	0.86	−0.55	−0.56	5s	2.89	4	3d	2.67	9
27	101449		0.35	0.65		−0.45	−0.68	5s	2.89	4	3d	2.67	9
28	101483	0.22	0.32	0.46	1.56	−0.21	−0.09				3d	2.67	9
29	101509	0.26	0.18	0.56	1.90	0.13	0.93				3d	2.68	9
30	101538		0.28	0.72		−0.35	−0.66				5s	2.89	3
31	101588		0.27	0.73		−0.48	−0.44				5s	2.90	3
32	101604		0.20	0.80		0.03	−0.25						
33	101637	0.39	0.28	0.32	1.86	−0.09	−0.09	5s(3d)	2.88(2.68)	5(11)			
34	101659		0.35	0.65		−0.58	−0.48	5s(3d)	2.88(2.68)	5(11)			
35	101690		0.40	0.60		−0.19	−0.52	5s(3d)	2.89(2.68)	5(11)			
36	101706		0.44	0.56		−0.33	−0.51	5s(3d)	2.89(2.69)	5(11)			
37	101737	0.12	0.43	0.45	1.00	−0.47	0.56	5s(3d)	2.89(2.69)	5(11)			
38	101769		0.62	0.38		−0.58	−0.47				5s	2.88	4
39	101804		0.30	0.70		−0.45	−0.58				5s	2.88	4
40	101826		0.43	0.57		−0.64	−0.41				5s	2.88	4
41	101916		0.22	0.78		−0.23	−0.73	5s	2.88	6			
42	101927		0.29	0.71		−0.20	−0.67	5s	2.88	6			
43	101966		0.39	0.61		−0.04	0.69				5s(3d)	2.87(2.69)	5(10)
44	102006		0.49	0.51		−0.45	−0.51				5s	2.87	5
45	102031		0.47	0.53		−0.11	−0.47				5s	2.87	5
46	102061	0.29		0.71	1.45		0.08	3d	2.69	12			
47	102095	0.12	0.36	0.52	0.60	−0.43	−0.22	5s(3d)	2.85(2.69)	7(12)			
48	102114		0.37	0.63		−0.45	−0.22	5s	2.85	7			
49	102171		0.57	0.43		−0.21	−0.07	5s	2.86	7			
50	102191		0.58	0.42		−0.58	0.53	5s	2.86	7	3d	2.68	11
51	102210		0.68	0.32		−0.46	0.26	5s	2.86	7	3d	2.68	11
52	102221		0.54	0.46		0.12	0.70	3d	2.67	13			
53	102234	0.60		0.40	1.94		1.10	3d	2.67	13			
54	102293	0.29	0.21	0.50	1.84	0.13	0.41	3d	2.68	13			
55	102322		0.56	0.44		−0.41	0.76	3d	2.68	13	5s	2.85	6
56	102353		0.58	0.42		−0.67	0.47	3d	2.68	13	5s	2.86	6
57	102422		0.40	0.60		−0.28	−0.10	5s	2.85	8			
58	102439		0.59	0.41		−0.46	−0.19	5s	2.86	8			
59	102466	0.13	0.50	0.37	0.90	−0.50	−0.16	5s	2.86	8	3d	2.67	12
60	102483	0.24	0.30	0.46	1.37	−0.14	0.22	5s	2.86	8	3d	2.67	12
61	102505	0.27	0.34	0.39	1.52	−0.25	1.15	5s	2.86	8	3d	2.68	12
62	102558		0.32	0.68		−0.35	−0.24				5s	2.85	7
63	102578		0.27	0.73		0.75	0.24	3d	2.68	14	5s	2.85	7
64	102597		0.52	0.48		0.91	0.94	3d	2.68	14	5s	2.85	7
65	102605		0.56	0.44		−0.24	0.77	3d	2.68	14	5s	2.85	7
66	102615		0.62	0.38		−0.53	1.29	3d	2.68	14	5s	2.85	7
67	102642		0.66	0.34		−0.42	0.93						
68	102660		0.56	0.44		−0.53	0.06						
69	102680		0.37	0.63		−0.21	−0.08						
70	102700		0.56	0.44		−0.45	0.46						
71	102728		0.52	0.48		−0.45	−0.16	5s	2.85	9			
72	102744		0.64	0.36		−0.44	−0.48	5s	2.86	9			

[a] The number sequentially indexes the photon energies used in the measurements. [b] The photon energy in cm^{-1} with uncertainty of ± 1 cm^{-1}. [c] Normalized branching ratios among $Cl^+(^3P_0)$, $Cl^+(^3P_1)$ and $Cl^+(^3P_2)$. The blanks in the column indicate the zero population. The uncertainty is ± 0.1. [d] The anisotropic parameter. The uncertainties are ± 0.15 for $Cl^+(^3P_0)$, and ± 0.10 for $Cl^+(^3P_1)$ and $Cl^+(^3P_2)$, respectively. [e] The $[A^2\Pi_{u,3/2}]$ and $[A^2\Pi_{u,1/2}]$ represent Rydberg series with ion-core $Cl_2^+(A^2\Pi_{u,3/2})$ and $Cl_2^+(A^2\Pi_{u,1/2})$, respectively. The n^* and v represent the effective principal quantum number for Rydberg state and the vibrational quantum number for the ion-core, respectively.

As we mentioned in the Introduction, the ion-pair yield spectra of Cl_2 in the range 13.26−13.73 eV are assigned from two Rydberg series, $[A^2\Pi_u]ns\sigma_g$, $^1\Pi_u$ (n = 6, 7), and $[A^2\Pi_u]nd\pi_g$, $^1\Sigma_u^+$ (n = 4, 5), respectively.[11] Therefore, it is natural to assign the ion-pair yield spectrum in the lower energy region by the same Rydberg series, however, with smaller effective principal numbers, or $[A^2\Pi_u]5s\sigma_g$,$^1\Pi_u$ and $[A^2\Pi_u]3d\pi_g$,$^1\Sigma_u^+$ for perpendicular and parallel transitions, respectively. All other possibilities are neglected, such as perpendicular transitions from $[A^2\Pi_u]3d\delta_g$,$^1\Pi_u$ and parallel transitions from $[A^2\Pi_{1/2,u}]5s\sigma_g$,$0_u^+$ in Hund's case (c) notation. We also only assigned the peaks at which we measured images. Table 2 shows the assignments along with other dynamical parameters discussed below.

To assign a peak to a particular Rydberg state in the spectrum, we used two criteria. First, the symmetry of the Rydberg state should conform to the observed symmetry from the imaging experiments. Second, the effective principal quantum numbers (n^*) calculated using eq (1) should be similar to those of Cl Rydberg atoms. The n^* for $[Cl^+]5s$ and $[Cl^+]3d$ Rydberg states range from 2.88 to 2.91 and 2.59 to 2.85, respectively, depending on the states of the ionic core.[25] It is found that the n^* in the range of 2.85−2.91 for $[A^2\Pi_u]5s\sigma_g$,$^1\Pi_u$ and 2.67−2.69 for $[A^2\Pi_u]3d\pi_g$,$^1\Sigma_u^+$ are the overall best in assigning the ion-pair yield spectrum, which also are in agreement with the values in the assignment of Rydberg series $[A^2\Pi_u]6s\sigma_g$,$^1\Pi_u$ and $[A^2\Pi_u]4d\pi_g$,$^1\Sigma_u^+$.[11]

It is seen from Figure 2 that the ion-pair yield spectrum is not rotationally and vibrationally resolved although the resolution of XUV laser is around 0.1 cm^{-1}, which indicates that the predissociations of Rydberg states are very fast. The ion-pair yield spectrum was obtained by recording the $^{35}Cl^-$ signals resulting from the dissociation of two isotopomers, $^{35}Cl_2$ and $^{35}Cl^{37}Cl$, with natural abundance of 9:6. In the assignments, a range of line positions has been assigned from the same vibrational bands with different quantum defects that may be regarded as from different rotational transitions or from different isotopomers.

B. Ion-Pair Dissociation Dynamics: Adiabatic State Correlation. The threshold for ion-pair dissociation of Cl_2 (E_{tipp}) is 11.833 eV.[10] In the range 12.41−12.72 eV, the following dissociation channels are possible:

$$Cl_2 \rightarrow Cl^+(^3P_{2,1,0}) + Cl^-(^1S_0) \quad (2)$$

The energy levels of $Cl^+(^3P_0)$ and $Cl^+(^3P_1)$ relative to $Cl^+(^3P_2)$ are 996 and 696 cm^{-1}, respectively. Figure 3 shows the experimental raw images of $^{35}Cl^-(^1S_0)$ at 72 different photon energies under the DC electric field. As we mentioned above, the available energy for the ion-pair dissociation is much larger than the red shift of the E_{tipp} due to the electric field, therefore, the electric field induced dissociation dynamics does not play an important role in this energy region.[2,7]

To obtain the dynamical information, the images were processed using our well-established procedures.[7−11] For examples, Figure 4 shows an expanded view of four raw images and quarters of 2-D slice images from the inverse Abel transform. Figures 5 and 6 show translational energy distributions and the angular distributions obtained from the 2-D slice images, respectively.

The anisotropic parameters β are obtained by applying the least-squares fitting method to the experimentally obtained angular distributions using the formula[26,27]

$$f(\theta) \propto 1 + \beta P_2(\cos\theta) \quad (3)$$

where θ is the angle between the recoil velocity and the polarization direction of the XUV laser, and $P_2(x)$ is the second order Legendre polynomial. In the limiting case of parallel or perpendicular transitions, β equals 2 or −1.

To obtain the angular distributions for $Cl^+(^3P_0)$, $Cl^+(^3P_1)$ and $Cl^+(^3P_2)$, we only integrate the signals inside the half-heights of their peaks or even narrower than these. Panels (a), (b) and (c) of Figure 7 show the β values for the production of $Cl^+(^3P_0)$, $Cl^+(^3P_1)$ and $Cl^+(^3P_2)$, respectively. To illustrate the changes of β values with the excitation photon energies, panel (d) of Figure 7 shows the ion-pair yield spectrum.

To obtain the branching ratios among $Cl^+(^3P_0)$, $Cl^+(^3P_1)$ and $Cl^+(^3P_2)$, a deconvolution method using Gaussian distribution functions has been applied to the translational energy distributions. Panels (a), (b) and (c) of Figure 8 show the branching ratios among fragments $Cl^+(^3P_0)$, $Cl^+(^3P_1)$ and $Cl^+(^3P_2)$, respectively, as a function of photon energies. Panel (d) of Figure 8 is the ion-pair yield spectrum showing the line positions for the measured branching ratios. At most of the excitation photon energies, the fragments $Cl^+(^3P_2)$ have the largest population among the three components, and the fragments $Cl^+(^3P_0)$ have the smallest population. At a number of excitation energies, fragments $Cl^+(^3P_0)$ are not populated at all. The applied photon energies, the β parameters and the branching ratios among $Cl^+(^3P_j)$ can be found in Table 2 using the index numbers.

As seen from Figure 7, the β values for fragments $Cl^+(^3P_0)$ are all positive, and in contrast with it, most of the fragments $Cl^+(^3P_1)$ have negative β values. For fragments $Cl^+(^3P_2)$, the β values have both positive and negative values that strongly depend on the excitation photon energies. Hence, the variation of β values for fragments $Cl^+(^3P_2)$ with the photon energies is in great contrast with the all positive β and mostly negative β for fragments $Cl^+(^3P_0)$ and $Cl^+(^3P_1)$, respectively. This fact may suggest two things: (1) strong product correlations may exist during the ion-pair dissociation for fragments $Cl^+(^3P_0)$ and $Cl^+(^3P_1)$; (2) the fragments $Cl^+(^3P_2)$ result from many closely adjacent electronic states with different symmetric properties.

The ion-pair dissociation is explained by the predissociation of Rydberg states. The experimental evidence for this are as follows: (1) the ion-pair yield spectrum shows some structures that can be assigned as the vibrational bands of Rydberg states, which was also pointed out by the previous publication;[22] (2) the excitation from the valence electronic states to ion-pair states involves a charge transfer process, if the direct transition to ion-pair states is the only mechanism, then we would only observe parallel transitions.[12−21] This is in contradiction with the experimental facts observed in this work. It is noted that a direct ion-pair dissociation mechanism cannot be ruled out for parallel transitions, however, the probability for it is low in our energy region as will be discussed below.

For diatomic molecules, the potential energy curves (PECs) are essential to understanding the dynamics of photodissociation. For Cl_2, the PECs for ion-pair states correlating with the production of $Cl^+(^3P_j) + Cl^-(^1S_0)$ and $Cl^+(^1D_2) + Cl^-(^1S_0)$ have been calculated in both $\Lambda-S$ (without spin−orbit coupling) and Ω (with spin−orbit coupling) approximations by Kokh et al.[12,13] In these calculations, the interactions of ion-pair states with low Rydberg states converging to $Cl_2^+(X^2\Pi_g)$ have been taken into account. All PECs show the typical double minimum structures due to the avoided crossings between Rydberg states and ion-pair states with the same symmetries. However, the adiabatic PECs of Rydberg states, $[A^2\Pi_u]5s\sigma_g$,$^1\Pi_u$ and $[A^2\Pi_u]3d\pi_g$,$^1\Sigma_u^+$ have not yet been reported.

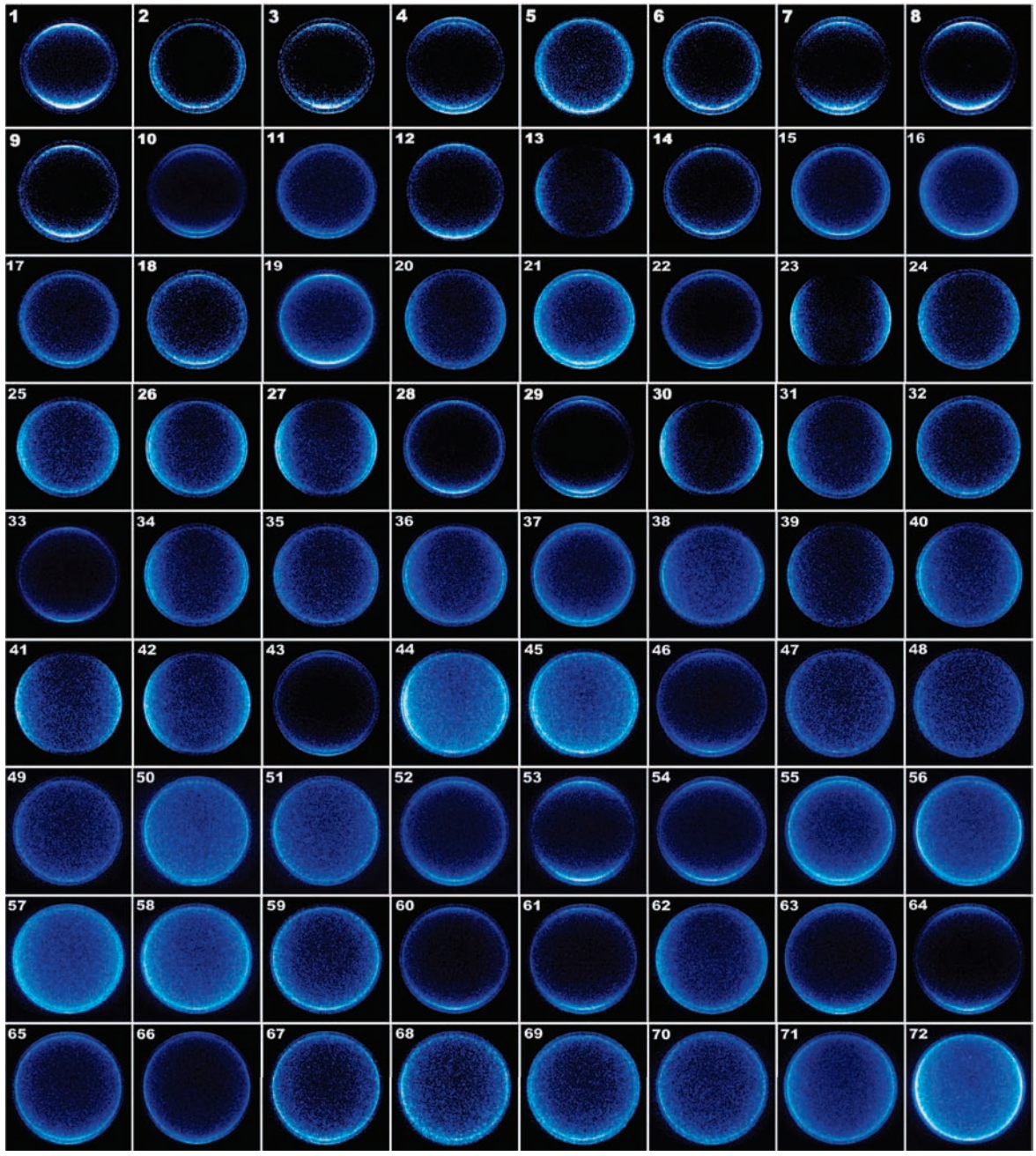

Figure 3. Velocity map images of Cl^- from the ion-pair dissociation of Cl_2. Each image has an index number at the upper left corner. The applied photon energies, the anisotropic parameters β, and the branching ratios among $Cl^+(^3P_0)$, $Cl^+(^3P_1)$ and $Cl^+(^3P_2)$ can be found in Table 2 using the index numbers. The polarization of XUV laser is in the imaging plane and along the up-and-down direction. The images were taken under the electric field strengths of ~850 V/cm for images 1 to 8, and ~700 V/cm for all others.

We have reported diabatic PECs of ion-pair states at the level of MRCI/CASSCF/avtz using the MOLPRO software package.[11,28] The diabatic means that the electronic configurations involving the Rydberg electron had not been included in the calculation of ion-pair states. Figure 9 shows such PECs with ungerade symmetry that may be excited by one-photon absorption. The PEC of Rydberg state $[A^2\Pi_u]5s\sigma_g,^1\Pi_u$ is also shown in Figure 9, which was obtained by shifting the PEC of $Cl_2^+(A^2\Pi_u)$ to the experimentally determined energy position. The PEC of $Cl_2^+(A^2\Pi_u)$ was also calculated at the level of MRCI/CASSCF/avtz. As pointed out by Kokh et al.,[13] the most noticeable feature of the PECs is that the state $1^1\Sigma_u^+$ correlating with channel for the production of $Cl^+(^1D_2)$ crosses both $1^3\Sigma_u^-$ and $2^3\Pi_u$ correlating with the channels of $Cl^+(^3P_j)$. A crossing between $1^3\Sigma_u^-$ and $2^3\Pi_u$ also occurs. In the Franck−Condon region, the state $1^1\Sigma_u^+$ has lower energy than the states $1^3\Sigma_u^-$ and $2^3\Pi_u$.

The main electronic configurations of ion-pair states at the Franck−Condon region are shown in Figure 10. From the electronic configurations of ion-pair states $1^3\Sigma_u^-$ and $2^3\Pi_u$, it is seen that direct excitations to them involve two-electron excitation processes, and hence have low transition probabilities. The direct excitation to $1^1\Sigma_u^+$ has a large transition dipole moment, which has already been observed in spectroscopic studies using photon energies ~8 eV.[19−21,29,30] However, for photon energies ~12.5 eV, the vertical excitation to $1^1\Sigma_u^+$ is out of the Franck−Condon region that is indicated in Figure 9 by the wave packet of the vibrational ground-state $Cl_2(X^1\Sigma_g^+)$, therefore, the direct ion-pair dissociation via $1^1\Sigma_u^+$ is difficult.

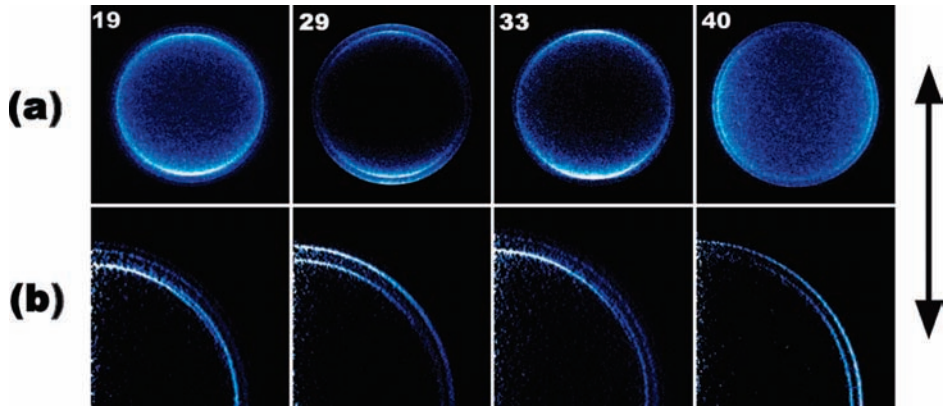

Figure 4. Four images of fragments Cl^- from the ion-pair dissociation of Cl_2. Panel (a) shows the experimental raw images, and panel (b) shows quarters of the 2-D slice images from the inverse Abel transforms of the raw images. The polarization of the XUV laser is indicated by the arrow on the right. The index number is at the upper left corner for each image. The images were taken under an electric field of ~700 V/cm. The brightness and contrast for each image have been adjusted in order to clearly show the different components of $Cl^+(^3P_j)$.

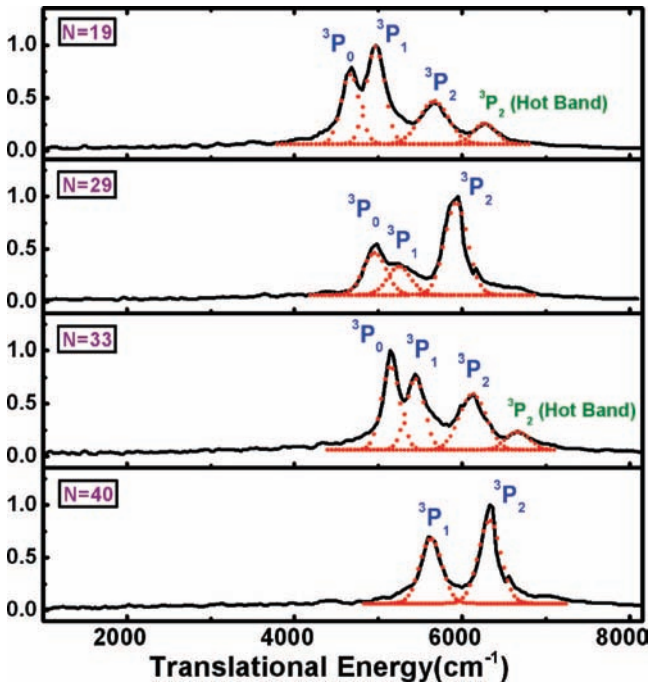

Figure 5. The center-of-mass translational energy distributions for ion-pair dissociation of Cl_2 at four excitation energies. The curves are fitted by convoluting Gaussian functions for translational energy distributions of different spin−orbit components, and the fittings are showed by dots.

The electronic configurations also play important role in the predissociation mechanism.[31] For ion-pair states $1^1\Sigma_u^+$, $1^3\Sigma_u^-$, and $2^3\Pi_u$, there are two and only two different electron orbitals between their electronic configurations and those of Rydberg series converging to the ion-core $Cl_2^+(A^2\Pi_u)$. This means that the predissociations between the three ion-pair states and the Rydberg series could occur via electrostatic perturbation. In another respect, the spin−orbit interaction requires that only one orbital is different between the two interacting states. This indicates that the probability of predissociation due to the spin−orbit perturbation between the ion-pair states and the Rydberg series converging to $Cl_2^+(A^2\Pi_u)$ is very rare.

From the above discussion, it is known that the predissociation of Rydberg states via ion-pair states $1^1\Sigma_u^+$, $1^3\Sigma_u^-$, and $2^3\Pi_u$ may be the most probable mechanism for the ion-pair dissociation. The interactions between the ion-pair states and Rydberg states are mainly from the electrostatic perturbation that requires the same set of good quantum numbers between the interacting states. It is better to describe both states using Hund's case (c) or approximation in which the projection of the total electronic angular momentum Ω on the molecular axis is a good quantum number. The Rydberg states, $[A^2\Pi_u]5s\sigma_g,^1\Pi_u$ and $[A^2\Pi_u]3d\pi_g,^1\Sigma_u^+$ have $\Omega = 1$ and 0, respectively. The PECs for ion-pair states in Hund's case (c) have been calculated by Kokh et al.[13] Figure 10 shows the ion-pair state correlation diagram based on their calculations. The avoided crossings due to the same symmetries are indicated as dots in the figure.

It is clear from Figure 10 that fragments $Cl^+(^3P_0)$ only correlate with the ion-pair state of $0_u^+(^3P_0)$ that is mainly from $2^3\Pi_u$ state. However, $0_u^+(^3P_0)$ consists of components from state mixing among $2^3\Pi_u$, $1^3\Sigma_u^-$ and $1^1\Sigma_u^+$. The ion-pair state $0_u^+(^3P_0)$ can only be predissociated by Rydberg state $[A^2\Pi_u]3d\pi_g,^1\Sigma_u^+$ ($\Omega = 0_u^+$) or, in other words, only parallel transitions are expected for the production of $Cl^+(^3P_0)$, which is in agreement with the experimental results.

For fragment $Cl^+(^3P_1)$, it correlates with $0_u^-(^3P_1)$ and $1_u(^3P_1)$ in which only $1_u(^3P_1)$ can interact with the Rydberg state of $[A^2\Pi_u]5s\sigma_g,^1\Pi_u$ ($\Omega = 1_u$). This means that fragment $Cl^+(^3P_1)$ should be only from perpendicular transition via homogeneous perturbation. The experimental results show that most of the fragments $Cl^+(^3P_1)$ do come from the perpendicular transitions, however, parallel transitions for $Cl^+(^3P_1)$ have been also observed for a small fraction of them. The mechanism for the parallel transition is proposed as following: (1) excitation to Rydberg state $[A^2\Pi_u]3d\pi_g,^1\Sigma_u^+$ that initializes a parallel transition, (2) interaction of the Rydberg state with ion-pair state $0_u^+(^3P_0)$ or $0_u^+(^3P_2)$, (3) heterogeneous perturbation or nonadiabatic interactions between $0_u^+(^3P_0)$ or $0_u^+(^3P_2)$ and $1_u(^3P_1)$ that produce fragment $Cl^+(^3P_1)$. The heterogeneous interaction is weak as shown by the experimental results.

For fragment $Cl^+(^3P_2)$, it correlates with $1_u(^3P_2)$ and $0_u^+(^3P_2)$ that are mainly from the ion-pair state $1^3\Sigma_u^-$. The $1_u(^3P_2)$ and $0_u^+(^3P_2)$ can interact with Rydberg states $[A^2\Pi_u]5s\sigma_g,^1\Pi_u\{\}$ and $[A^2\Pi_u]3d\pi_g,^1\Sigma_u^+$, respectively. It is therefore anticipated that both parallel and perpendicular transitions should be allowed. The changes of β parameters or the transitions properties for the production of $Cl^+(^3P_2)$ reflect that different Rydberg states are excited at different photon energies in the ion-pair yield spectrum. The reason for large population of $Cl^+(^3P_2)$ relative to those of $Cl^+(^3P_{0,1})$ is that there is better overlap of the vibrational wave functions between ion-pair state $1^3\Sigma_u^-$ that

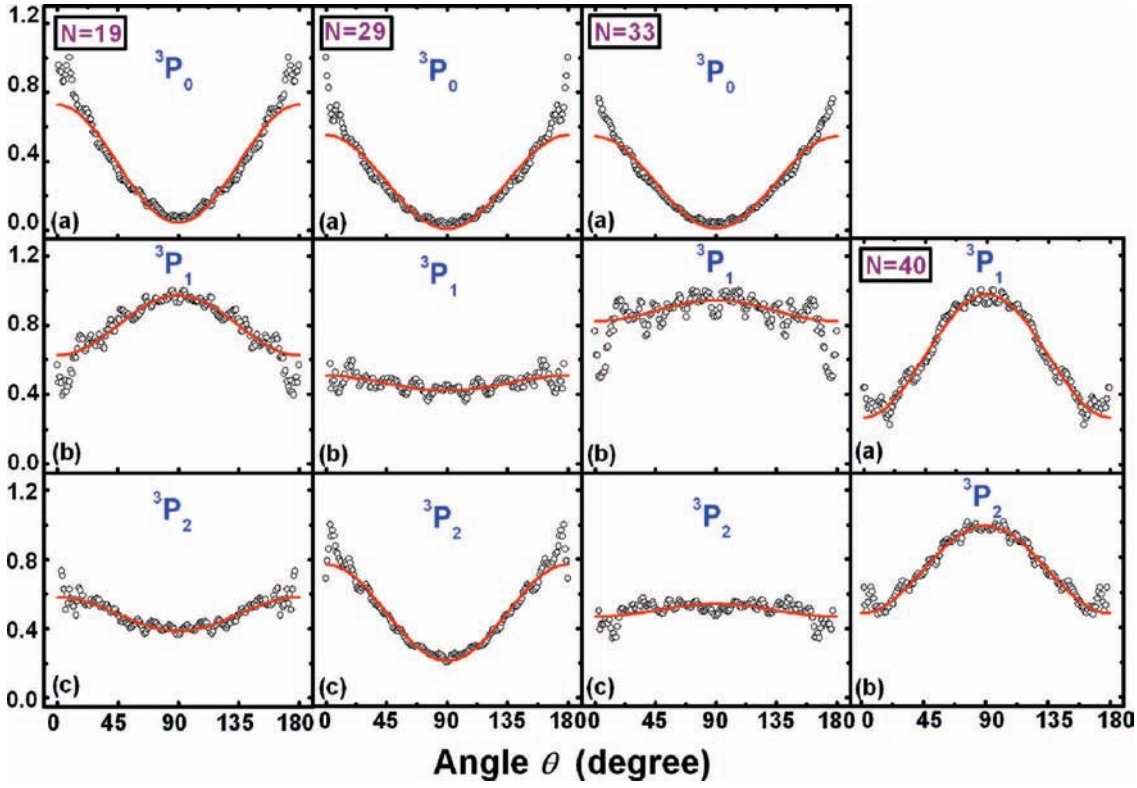

Figure 6. Angular distributions of Cl^- fragments from the ion-pair dissociation of Cl_2 at four excitation energies. The small circles represent the experimental data, and the solid curves are the least-squares fittings using eq (3). The noises near 0 and 180 degrees are from Abel transforms, which have not been included in the fittings.

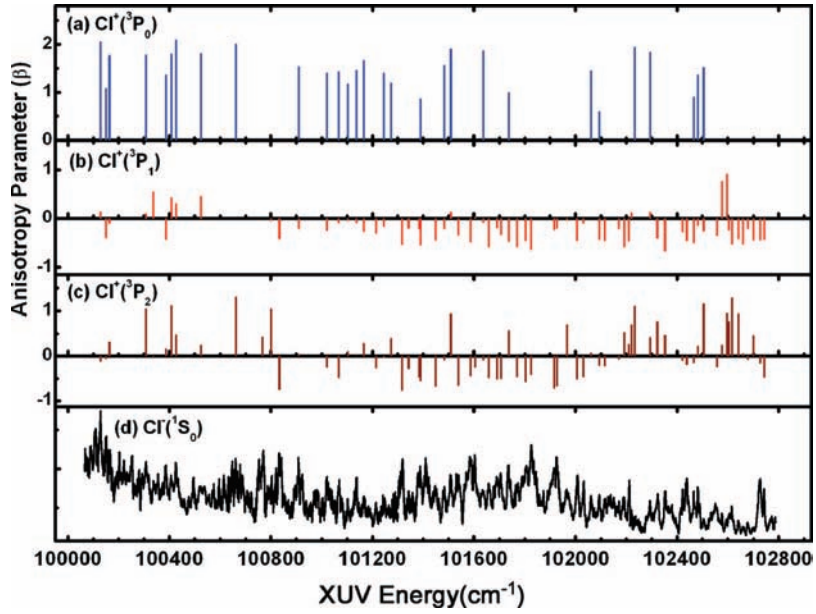

Figure 7. The anisotropic parameters β of Cl^- fragments for the ion-pair dissociation of Cl_2. Panel (a), (b) and (c) are for $Cl^+(^3P_0)$, $Cl^+(^3P_1)$ and $Cl^+(^3P_2)$, respectively. Panel (d) is the ion-pair yield spectrum showing the relative energy positions of β.

makes up the main components of $Cl^+(^3P_2)$ and the Rydberg states, as shown in Figure 9.

Although the ion-pair dissociations of Cl_2 occur in the energy region in which high density of Rydberg states exists, the experimental results show that the perturbations between Rydberg states and ion-pair states are mainly from the electrostatic perturbations, and the dissociations occur in favor of the conservation of Ω, the projection of total electronic angular momentum on the molecular axis.

C. Examples: Dynamics at Four Photon Energies. The above discussion about the dynamics based on the assignment of Rydberg states and adiabatic state correlation is able to explain qualitatively most of the images observed. However, for a small number of photon energies ($N = 2$, 15, 16, 20, 21, 32, 67−70), the excited states could not be assigned from the Rydberg series of $[A^2\Pi_u]5s\sigma_g,{}^1\Pi_u$ and $[A^2\Pi_u]3d\pi_g,{}^1\Sigma_u^+$. Further work is needed to assign these peaks. Here, we apply our above discussion to four example images (Figure 4) at the excitation energies for which the Rydberg states have been assigned.

A careful look at the 2-D slices in Figure 4 shows that there are actually four rings for images $N = 19$, 29, and 33. The largest rings are from the ion-pair dissociation of the first

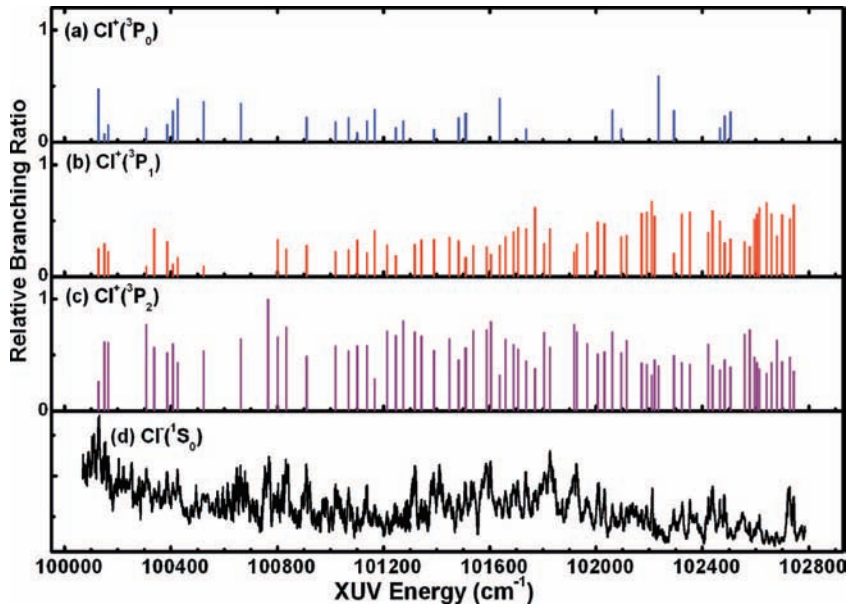

Figure 8. The branching ratios among the fragments $Cl^+(^3P_0)$, $Cl^+(^3P_1)$ and $Cl^+(^3P_2)$ for ion-pair dissociation of Cl_2. The total intensity is assumed to be unity at each photon energy. Panels (a), (b) and (c) are intensities of $Cl^+(^3P_0)$, $Cl^+(^3P_1)$ and $Cl^+(^3P_2)$, respectively. Panel (d) is the ion-pair yield spectrum showing the relative energy positions of the measured branching ratios.

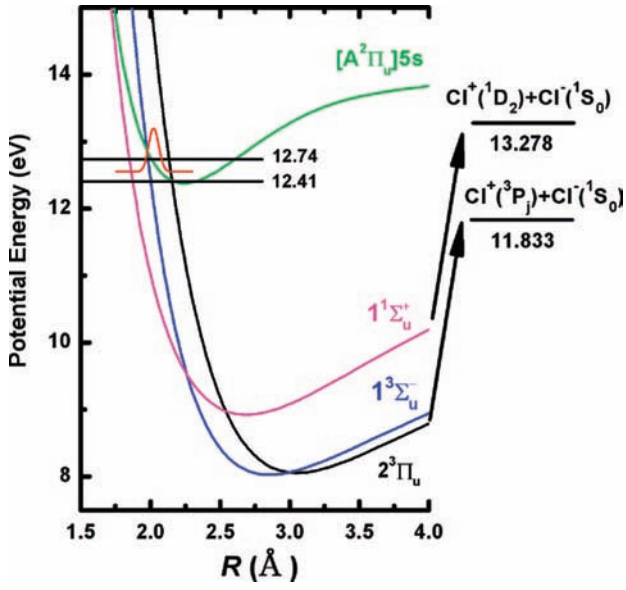

Figure 9. The diabatic ion-pair PECs of Cl_2 calculated at the level of MRCI/CASSCF/avtz.[11] The diabatic means that the electronic configurations involving the Rydberg electron had not been included in the calculation. The PEC of Rydberg state $[A^2\Pi_u]5s$ is obtained by shifting that of $Cl_2^+(A^2\Pi_u)$ to the experimentally determined energy position, 12.38 eV. The wave packet for the vibrational ground-state of $Cl_2(X^1\Sigma_g^+)$ is also shown in the figure to indicate the Franck−Condon region.

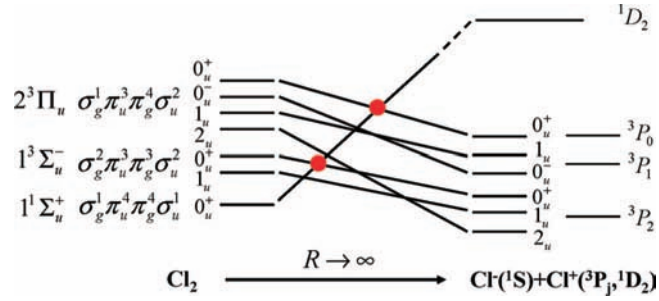

Figure 10. The adiabatic state correlation diagram for ion-pair dissociation of Cl_2 based on the multiconfiguration *ab initio* calculations including spin−orbit perturbation by Kokh et al.[13] The small dots in the diagram indicate the avoided crossings due to the adiabatic interaction among 0_u^+ states.

vibrational excited-state of $Cl_2(v = 1)$. We will not discuss the dynamics related with the hot band in this work.

(i) For $h\nu = 101167$ cm^{-1} ($N = 19$), this peak is assigned from two simultaneously excited Rydberg states: $[A^2\Pi_{u,1/2}]3d\pi_g,{}^1\Sigma_u^+$ with $v = 8$, $n^* = 2.68$ and $[A^2\Pi_{u,3/2}]5s\sigma_g,{}^1\Pi_u$ with $v = 3$, $n^* = 2.91$. The β values for fragments $Cl^+(^3P_0)$, $Cl^+(^3P_1)$ and $Cl^+(^3P_2)$ are 1.67, −0.27 and 0.29, and the branching ratios for them are 0.30, 0.41, and 0.29, respectively. The fragments $Cl^+(^3P_0)$ and $Cl^+(^3P_2)$ derive mainly from the predissociation of Rydberg state $[A^2\Pi_{u,1/2}]3d\pi_g$, $^1\Sigma_u^+$, and the fragments $Cl^+(^3P_1)$ derive mainly from the predissociations of Rydberg state $[A^2\Pi_{u,3/2}]5s\sigma_g$, $^1\Pi_u$.

(ii) For $h\nu = 101509$ cm^{-1} ($N = 29$), this peak is assigned from Rydberg state $[A^2\Pi_{u,1/2}]3d\pi_g$, $^1\Sigma_u^+$ with $v = 9$, and $n^* = 2.68$. The β values for fragments $Cl^+(^3P_0)$, $Cl^+(^3P_1)$, and $Cl^+(^3P_2)$ are 1.90, 0.13 and 0.93, and the branching ratios for them are 0.26, 0.18 and 0.56, respectively. The fragments $Cl^+(^3P_0)$, $Cl^+(^3P_1)$ and $Cl^+(^3P_2)$ derive mainly from predissociation of Rydberg state $[A^2\Pi_{u,1/2}]3d\pi_g$, $^1\Sigma_u^+$ that can interact with ion-pair states of $0_u^+(^3P_0)$ and $0_u^+(^3P_2)$. For fragments $Cl^+(^3P_1)$, it is expected that heterogeneous perturbations between $1_u(^3P_1)$ and $0_u^+(^3P_0)$ or $0_u^+(^3P_2)$ occur, which produce fragments $Cl^+(^3P_1)$. However, as shown by the branching ratios among the three spin−orbit components, this probability is low.

(iii) For $h\nu = 101637$ cm^{-1} ($N = 33$), this peak is assigned from two simultaneously excited Rydberg states: $[A^2\Pi_{u,3/2}]3d\pi_g,{}^1\Sigma_u^+$ with $v = 11$, $n^* = 2.68$ and $[A^2\Pi_{u,3/2}]5s\sigma_g,{}^1\Pi_u$ with $v = 5$, $n^* = 2.88$. The β values for fragments $Cl^+(^3P_0)$, $Cl^+(^3P_1)$, and $Cl^+(^3P_2)$ are 1.86, −0.09 and −0.09, and the branching ratios for them are 0.39, 0.28, and 0.32, respectively. The fragments $Cl^+(^3P_0)$ derive mainly from the predissociation of Rydberg state $[A^2\Pi_{u,1/2}]3d\pi_g,{}^1\Sigma_u^+$, the fragments $Cl^+(^3P_2)$ derive from the predissociation of Rydberg state $[A^2\Pi_{u,3/2}]5s\sigma_g,{}^1\Pi_u$ and $[A^2\Pi_{u,3/2}]3d\pi_g,{}^1\Sigma_u^+$ with almost equal probabilities. For fragments $Cl^+(^3P_1)$, in addition to predissociations from $[A^2\Pi_{u,3/2}]5s\sigma_g,{}^1\Pi_u$, the predissociations of $[A^2\Pi_{u,3/2}]3d\pi_g,{}^1\Sigma_u^+$ by $0_u^+(^3P_0)$

or $0_u^+(^3P_2)$ and their heterogeneous interactions with $1u(^3P_1)$ should occur, which produce almost half of the fragments $Cl^+(^3P_0)$.

(iv) For $h\upsilon = 101826\ cm^{-1}$ ($N = 40$), this peak is assigned from Rydberg states $[A^2\Pi_{u,1/2}]5s\sigma_g,^1\Pi_u$ with $\upsilon = 4$, and $n^* = 2.88$. The β values for fragments $Cl^+(^3P_1)$ and $Cl^+(^3P_2)$ are -0.64 and -0.41, and the branching ratios for them are 0.43 and 0.57, respectively. As seen from Figure 4, only two rings corresponding to $Cl^+(^3P_1)$ and $Cl^+(^3P_2)$ exist, and they are both from perpendicular transition. The fragments $Cl^+(^3P_1)$ and $Cl^+(^3P_2)$ derive mainly from predissociation of Rydberg state $[A^2\Pi_{u,1/2}]5s\sigma_g,^1\Pi_u$.

IV. Summary and Conclusion

We have studied the ion-pair dissociation dynamics of Cl_2 in the range 12.41−12.74 eV using XUV laser and velocity map imaging method. The ion-pair yield spectrum has been measured, and 72 velocity map images of $Cl^-(^1S_0)$ have been recorded for the peaks in the spectrum. From the images, the branching ratios among $Cl^+(^3P_2)$, $Cl^+(^3P_1)$ and $Cl^+(^3P_0)$, and their corresponding anisotropic parameters β have been determined. The ion-pair dissociation dynamics is explained by the predissociation of Rydberg states converging to ion-core $Cl_2^+(A^2\Pi_u)$. The $Cl^-(^1S_0)$ ion-pair yield spectrum has been assigned based on the symmetric properties of Rydberg states determined in the imaging experiments. For the production of $Cl^+(^3P_0)$, it is found that all of them are from parallel transitions correlating with the predissociation of Rydberg state $[A^2\Pi_u]3d\pi_g,^1\Sigma_u^+$. But for $Cl^+(^3P_1)$, most of them are from perpendicular transitions correlating with the predissociation of $[A^2\Pi_u]5s\sigma_g,^1\Pi_u$. The production of $Cl^+(^3P_2)$ is the major channel in this energy region, and they come from both parallel and perpendicular transitions correlating with Rydberg states $[A^2\Pi_u]3d\pi_g,^1\Sigma_u^+$ and $[A^2\Pi_u]5s\sigma_g,^1\Pi_u$, respectively. Based on the experimental results and the adiabatic state correlation diagram, it is found that the projection of the total electronic angular momentum on the molecular axis (Ω) is conserved for fragment $Cl^+(^3P_0)$, and is nearly conserved for fragment $Cl^+(^3P_1)$. The ion-pair dissociation may be regarded as a probe for the symmetric properties of Rydberg states.

Acknowledgment. The authors are grateful to Ms. Shuming Gao for her assistance in experiments. This work is funded by Projects 20673066, 20773076, and 10734040 supported by the National Science Foundation of China, and Project 2007CB815200 supported by NKBRSF of China, the National High-Tech ICF Committee of China, and the Chinese Research Association of Atomic and Molecular Data.

References and Notes

(1) Hatano, Y. *J. Electron Spectrsoc. Relat. Phenom.* **2001**, *119*, 107.
(2) Reinhold, E.; Ubachs, W. *Mol. Phys.* **2005**, *103*, 1329.
(3) Suit, A. G.; Hepburn, J. W. *Annu. Rev. Phys. Chem.* **2006**, *57*, 431.
(4) Suto, K.; Sato, Y.; Reed, C. L.; Skorokhodov, V.; Matsumi, Y.; Kawasaki, M. *J. Phys. Chem. A* **1997**, *101*, 1222.
(5) Li, W.; Lucchese, R. R.; Doyuran, A.; Wu, Z.; Loos, H.; Hall, G. E.; Suits, A. G. *Phys. Rev. Lett.* **2004**, *92*, 083002.
(6) Xu, D.; Huang, J.; Price, R. J.; Jackson, W. M. *J. Phys. Chem. A* **2004**, *108*, 9916.
(7) Hao, Y; Zhou, C.; Mo, Y. *J. Phys. Chem. A* **2005**, *109*, 5832.
(8) Hao, Y; Zhou, C.; Mo, Y. *J. Phys. Chem. A* **2007**, *111*, 10887.
(9) Yang, J.; Hao, Y.; Li, J.; Zhou, C.; Mo, Y. *J. Chem. Phys.* **2005**, *122*, 134308.
(10) Li, J.; Hao, Y.; Zhou, C.; Yang, J.; Mo, Y. *J. Chem. Phys.* **2007**, *127*, 104307.
(11) Hao, Y.; Zhou, C.; Mo, Y. To be submitted.
(12) Peyerimhoff, S. D.; Buenker, R. J. *Chem. Phys.* **1981**, *57*, 279.
(13) Kokh, D. B.; Alekseyev, A. B.; Buenker, R. J. *J. Chem. Phys.* **2001**, *115*, 9298.
(14) Si, J.-H.; Ishiwata, T.; Obi, K *J. Mol. Spectrosc.* **1991**, *147*, 33.
(15) Ishiwata, T.; Kasai, Y.; Obi, K. *J. Chem. Phys.* **1993**, *98*, 3620.
(16) Ishiwata, T.; Shinzawa, T.; Si, J.-H.; Obi, K.; Tanaka, T. *J. Mol. Spectrosc.* **1994**, *166*, 321.
(17) Ishiwata, T.; Kasai, Y.; Obi, K. *Chem. Phys. Lett.* **1996**, *261*, 175.
(18) Al-Kahali, M. S. N.; Donovan, R. J.; Lawley, K. P.; Min, Z.; Ridley, T. *J. Chem. Phys.* **1996**, *104*, 1825.
(19) Yamanouchi, K.; Tsuchizawa, T.; Miyawaki, J.; Tsuchiya, S. *Chem. Phys. Lett.* **1989**, *4*, 301.
(20) Nee, J. B. *J. Phys. B: At. Mol. Opt. Phys.* **1990**, *23*, 3325.
(21) Tsuchizawa, T.; Yamanouchi, K.; Tsuchiya, S. *J. Chem. Phys.* **1990**, *93*, 111.
(22) Berkowitz, J.; Mayhew, C. A.; Ruscic, B. *Chem. Phys.* **1988**, *123*, 317.
(23) Eppink, A. T. J. B; Parker, D. H. *Rev. Sci. Instrum.* **1997**, *68*, 3477.
(24) Tuckett, R. P.; Peyerimhoff, S. D. *Chem. Phys.* **1984**, *83*, 203.
(25) Cantu, A. M.; Parkinson, W. H.; Grisendi, T.; Tagliaferri, G. *Phys. Scr.* **1985**, *31*, 579.
(26) Zare, R. N.; Herschbach, R. D. *Proc. IEEE* **1963**, *51*, 173.
(27) Mo, Y.; Suzuki, T. *J. Chem. Phys.* **2000**, *112*, 3463.
(28) MOLPRO, version 2006.1, a package of *ab initio* programs: Werner, H. J.; Knowles, P. J.; Lindh, R.; Manby, F. R.; Schutz, M. See: http://www.molpro.net.
(29) Wang, P.; Okuda, I. V.; Dimov, S. S; Lipson, R. H. *J. Mol. Spectrosc.* **1998**, *190*, 213.
(30) Wang, P.; Okuda, I. V.; Dimov, S. S; Lipson, R. H. *Chem. Phys. Lett.* **1994**, *229*, 370.
(31) Lefebvre-Brion, H.; Field, R. W. *The Spectra and Dynamics of Diatomic Molecules*; Elsevier Academy Press: Amsterdam, 2004.

JP804272W